Eur. Phys. J. C (2022) 82:891
https://doi.org/10.1140/epjc/s10052-022-10859-z

THE EUROPEAN PHYSICAL JOURNAL C

Regular Article - Experimental Physics

# Long term measurement of the $^{222}$Rn concentration in the Canfranc Underground Laboratory

**J. Amaré[1,2], I. Bandac[2], A. Blancas[1], S. Borjabad[2], S. Buisán[3], S. Cebrián[1,2,5], D. Cintas[1,2], I. Coarasa[1,2], E. García[1,2,5], M. Martínez[1,2,4], R. Núñez-Lagos[5], M. A. Oliván[1], Y. Ortigoza[5,6], A. Ortiz de Solórzano[1,2,5], C. Pérez[1,2,5], J. Puimedón[1,2,5,a], S. Rodríguez[5], A. Salinas[1,2], M. L. Sarsa[1,2], P. Villar[1]**

[1] Centro de Astropartículas y Física de Altas Energías (CAPA), Universidad de Zaragoza, Pedro Cerbuna 12, 50009 Zaragoza, Spain
[2] Laboratorio Subterráneo de Canfranc, Paseo de los Ayerbe s/n, 22880 Canfranc Estación, Huesca, Spain
[3] AEMET, Delegación Territorial de AEMET en Aragón, Paseo del Canal 17, 50007 Zaragoza, Spain
[4] Fundación ARAID, Avenida de Ranillas 1D, 50018 Zaragoza, Spain
[5] Laboratorio de Bajas Actividades (LABAC), Universidad de Zaragoza, Pedro Cerbuna 12, 50009 Zaragoza, Spain
[6] EUPLA, Calle Mayor 5, 50100 Zaragoza, La Almunia de Doña Godina, Spain

Received: 30 March 2022 / Accepted: 27 September 2022


**Abstract** We report the results of 6 years (2013–2018) of measurements of $^{222}$Rn air concentration, relative humidity, atmospheric pressure and temperature in the halls A, B and C of the Canfranc Underground Laboratory (LSC). We have calculated all the Pearson correlation coefficients among these parameters and we have found a positive correlation between the $^{222}$Rn concentration and the relative humidity. Both correlated variables show a seasonal periodicity. The joint analysis of laboratory data and 4 years (2015–2018) of the meteorological variables outside the laboratory shows the correlation between the $^{222}$Rn concentration and the outside temperature. The collected information stresses the relevance of designing good Rn-mitigation strategies in current and future experiments at LSC; in particular, we have checked for two years (2017–2018) the good performance of the mitigation procedure of the ANAIS-112 experiment. Finally, we have monitored (2019–2021) for 2 years of live time, the radon-free air provided by the radon abatement system installed in the laboratory.

## 1 Introduction

Monitoring the level of $^{222}$Rn in laboratories of low activity measurements and, in particular, in underground laboratories is essential to ensure the safety of the workers inside the laboratory. The main remediation action is a correct ventilation [1–4] to evacuate the radon emanation from the rock and to keep a concentration similar to that of the open air, that usually is $< 100$ Bq m$^{-3}$ [5]. The posterior actions to provide a very low radioactive background to the experiments in the laboratory depend on their requirements. The experiments can be purged with nitrogen (from compressed nitrogen or evaporated from a liquid nitrogen dewar) or with radon-free air provided that the laboratory has an adequate system to satisfy this demand, see for instance [6]. Monitoring the $^{222}$Rn level is also very important to avoid the plate-out of the $^{222}$Rn progeny, specially $^{210}$Pb, during the assembly of the components of an experiment [7]. The seasonal modulation of the $^{222}$Rn concentration affects specially to experiments aiming at the study of the annual modulation expected in the interaction rate of the galactic halo dark matter particles [8]. Because of that, these experiments [9,10] are specifically isolated from the laboratory air and conveniently purged with radon free gas.

We address three items in this article: monitoring the $^{222}$Rn concentration inside the LSC and its correlation with the internal and external temperature, pressure and relative humidity; monitoring the residual $^{222}$Rn concentration of the evaporated nitrogen that was used to purge the ANAIS-112 experiment during 2017–2018 [11,12] and, finally, monitoring the air provided by the radon abatement system [6] that supplies radon-free air to the experiments in the LSC [13–19]. Our data add very useful information to the published results of other background sources at LSC: the rock radioactivity [20], the neutron flux [21,22] and the cosmic-ray muon flux [23].

[a] e-mail: puimedon@unizar.es (corresponding author)

Published online: 08 October 2022

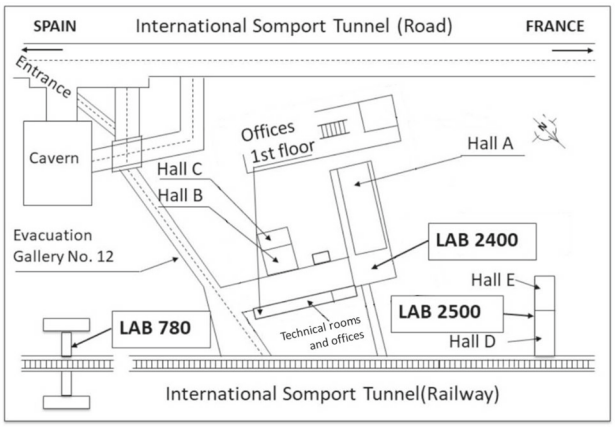


**Fig. 1** Scheme (not to scale) of the Canfranc Underground Laboratory facilities

## 2 Description of the Canfranc Underground Laboratory

The Canfranc Underground Laboratory, LSC[1] (Laboratorio Subterráneo de Canfranc) is a Spanish scientific installation located in Aragón, in the village Canfranc-Estación (Huesca) at 1120 m above sea level (geographical coordinates: 42° 46′ 30″ N; 0° 31′ 42″ W). Its laboratories and rooms have been excavated in the rock at 800 m depth, below the Tobazo Mountain, at the Spanish Pyrenees between the Somport road tunnel, which links Spain with France, and the parallel railway tunnel today in disuse.

The underground infrastructure has a total surface of about 1600 $m^2$ divided in LAB780 (two small experimental rooms at 260 m depth), LAB2400 and LAB2500 (both at 800 m depth), named according to the distance in meters from each location to the Spanish entrance of the railway tunnel (780, 2400 and 2500 m, respectively). This work has focused on the main experimental area (LAB2400) that consists of a large room, hall A, $40 \times 15 \times 12$ (height) $m^3$ and a smaller volume of $15 \times 10 \times 8$ (height) $m^3$ divided into two contiguous rooms, halls B and C (Fig. 1).

The ventilation provides around 11,000 $m^3\ h^{-1}$ of fresh air. The flow of fresh air is taken from the mountain at 1400 m altitude and then reaches an intermediate ventilation room at 1120 m through a ventilation shaft and a ventilation gallery excavated in the rock. From there it is sent to the air conditioning room by a forced ventilation duct, where it joins 14,000 $m^3\ h^{-1}$ of the returned air and its final temperature is regulated by the air conditioning system. The fresh air flow guarantees the total renewal of the laboratory air once per hour [24].

**Table 1** Annual average activity concentration of $^{222}$Rn (Bq $m^{-3}$) from 2013 to 2018. Their statistical uncertainties are approximately 0.07% whereas the instrument calibration error is 3%. The last column is the annual average for the 6 years of data

| Room | 2013 | 2014 | 2015 | 2016 | 2017 | 2018 | 2013-8 |
|---|---|---|---|---|---|---|---|
| Hall A | 87.5 | 82.4 | 82.8 | 80.4 | 80.8 | 82.9 | 82.8 |
| Hall B | 89.1 | 83.8 | 84.0 | 82.8 | 84.8 | 87.0 | 85.2 |
| Hall C | 89.2 | 82.7 | 86.1 | 82.9 | 83.3 | 84.4 | 84.8 |

## 3 $^{222}$Rn concentration in 6 years of data

The here reported measurements[2] of the $^{222}$Rn concentration in air ($Rn_i$), the temperature ($T_i$), the atmospheric pressure ($P_i$) and the relative humidity ($RH_i$) have been obtained using three Genitron (now BERTIN) ALPHAGUARD P30™ monitors from 2013 to 2018. The measurements were taken continuously by a dedicated software that recorded every 10 min the values of the four variables and the statistical uncertainty of the $^{222}$Rn concentration. Though the monitor does not distinguish $^{220}$Rn from $^{222}$Rn, their respective half-lives (56 s and 3.8 days) imply that the concentration of $^{220}$Rn in the laboratory is $2 \times 10^{-4}$ that of $^{222}$Rn, assuming secular equilibrium in $^{232}$Th and $^{238}$U chains and the same activity of $^{238}$U and $^{232}$Th for the mean rock [25]. The $^{220}$Rn concentration would be important if the rock and soils at Canfranc, as well as the concrete used for the laboratory walls, were thorium bearing minerals. The observed U/Th ratios of the rock at Canfranc tunnel [20], of the soils in the region close to Canfranc [26] and of the concrete, support the negligible contribution of $^{220}$Rn to the monitor measurements.

The calibration uncertainties quoted in the data sheet are 3% for the $^{222}$Rn concentration activity, 1.5 °C for the temperature, 3 hPa for the atmospheric pressure and 3% for the relative humidity. The calibrations of the monitors were tested by an interlaboratory comparison in 2015 [27]. The mean departure of our monitors was a 9% with respect to the $^{222}$Rn concentrations measured by the reference monitor of the comparison.

The $^{222}$Rn annual average activity concentrations in the three halls are listed in Table 1; their statistical uncertainties are about 0.07% because the response of the monitor is (5 counts per minute)/(100 Bq $m^{-3}$). The radon annual level is independent of the hall (within the 3% instrument calibration uncertainty), it complies with the European directive on radon in workplaces [28], with the ICRP recommendations [29] and it is well below the 600 Bq $m^{-3}$ allowed by Spanish legislation [30].

[1] Detailed information at www.lsc-canfranc.es.

[2] The subscript "i" refers to the variables inside LSC.

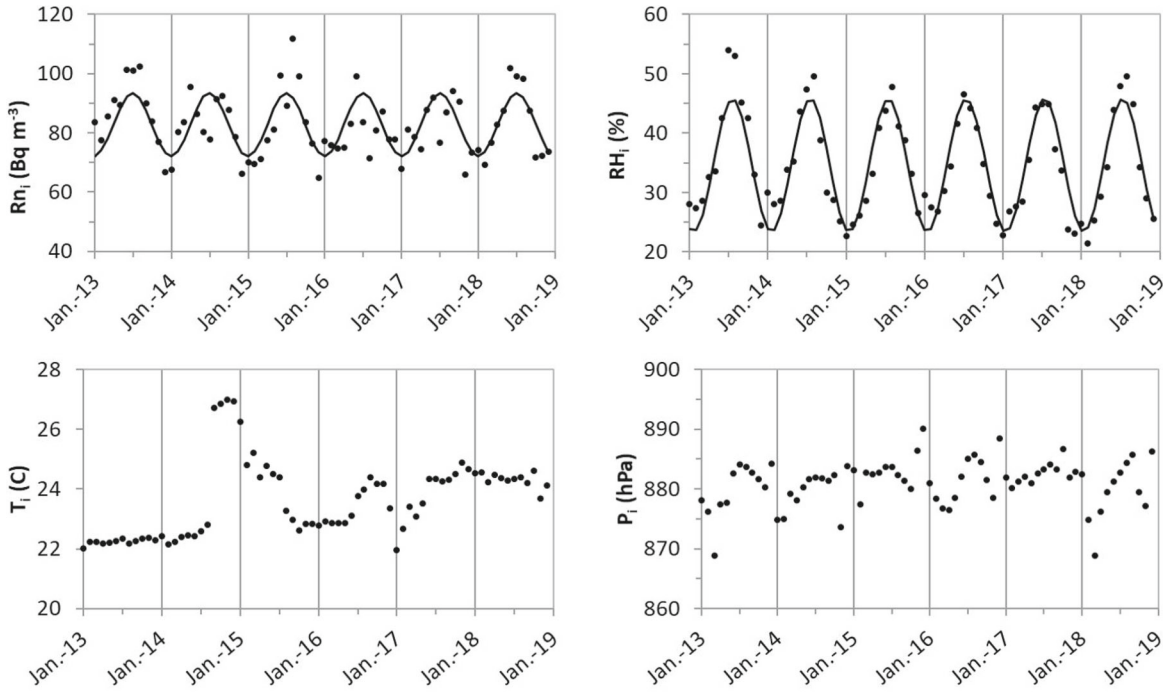


**Fig. 2** Monthly average of the hall A data: $^{222}$Rn concentration (upper left), relative humidity (upper right), temperature (bottom left) and atmospheric pressure (bottom right) from January 2013 to December 2018. The fits of the $^{222}$Rn concentration and the relative humidity to Eq. 2 are also shown. Corresponding plots for halls B and C are similar, except the temperature (see Fig. 3)

### 3.1 Correlations between the variables inside the laboratory

The relations between meteorological parameters and levels of $^{222}$Rn have been studied before at shallow depth, see for instance [31]. In this section, we give the results for all possible correlations between every pair of the monthly averages at LSC ($^{222}$Rn concentration, temperature, atmospheric pressure and relative humidity). Figure 2 plots the monthly averages of these four parameters for the 6 years for the hall A. Halls B and C have very similar plots, except for the temperature (Fig. 3) due to the liquefaction [32] of the argon needed for the ArDM experiment, that increased the temperature of the hall A (Fig. 2). The liquefaction in hall A started on 2 September 2014 using three cryocoolers. On 15 January 2015 one of the cryocoolers was turned off and the process continued for several months. The temperature increase in halls B and C is much smaller than in hall A (Fig. 3) due to the distance (Fig. 1) and the ventilation system working in hall A.

The statistical uncertainty of the $^{222}$Rn monthly average is 0.24% and those of the other three variables are unknown because of the lack of information in the data sheet of the radon monitor, though likely they are less than their calibration uncertainties. The relative humidity has a clear seasonal periodicity and the $^{222}$Rn concentration points to a similar behaviour, more evident in 2013, 2015 and 2018.

Table 2 shows the values of the Pearson correlation coefficient, $r$, for the monthly averages of all the pairs of parameters measured at halls A, B and C.

The statistical significance of the $r$-value of $n$ pairs of two variables can be easily calculated because the variable

$$t = r\sqrt{\frac{n-2}{1-r^2}} \tag{1}$$

follows the Student's $t$ distribution with $n-2$ degrees of freedom for two uncorrelated normal variables [33]. Even in the case of non-normal variables or small size $n$, the Student's $t$-distribution is a very good approximation for the $t$ variable in Eq. (1) [34]. Therefore, the decision threshold, $|r_\alpha|$, to reject the null hypothesis (no correlation) is obtained from the corresponding two-tailed $|t_\alpha|$.

We take a 99.92% CL for the decision threshold because if the variables of Table 2 are uncorrelated, the probability to get some $r$-value $\ni |r| > |r_\alpha|$ with 66 evaluated $r$-values is $1-(0.9992)^{66} = 0.05$, similar to a 95% CL if only one $r$-value were evaluated. The monthly average 6-year data gives $n = 72$, i.e., 70 degrees of freedom for the Student's $t$ and $|r_{\alpha=0.0008}| = 0.39$.

The $^{222}$Rn concentration in halls A, B and C are highly correlated, $r = 0.94$ to 0.98, and similar behaviour can be found for the pressure and the relative humidity. The temperature behaviour is different: there is correlation between the contiguous halls B and C, $r = 0.86$; the halls A and B are slightly correlated, $r = 0.53$; meanwhile the halls A and C are uncorrelated, $r = 0.32$, because halls B and C were not very affected by the argon liquefaction of the ArDM experiment. There is also correlation between the relative humidity

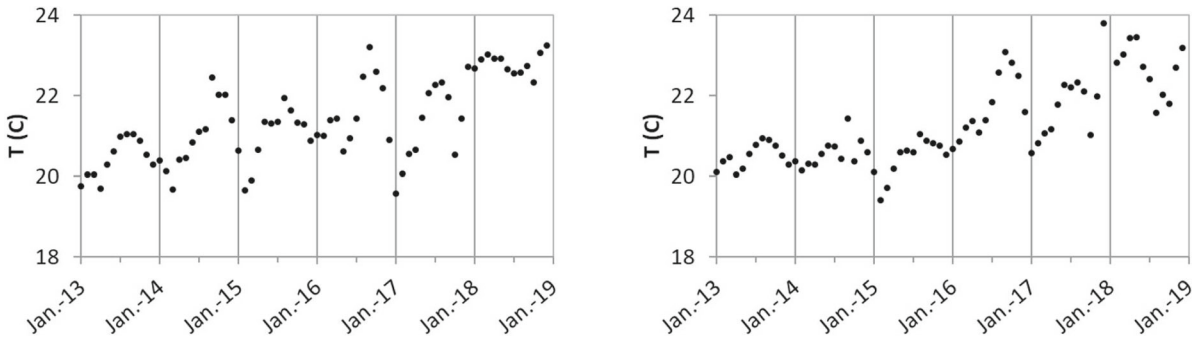


**Fig. 3** Monthly average of the temperature in the hall B (left) and hall C (right) from January 2013 to December 2018. The sharp increase of the temperature due to ArDM experiment (see text) is very attenuated in the hall B and it is almost imperceptible in the hall C

**Table 2** Values of Pearson correlation coefficient $r$ (2013–18) for all pairs of the measured monthly averaged parameters inside the LSC

| | | Radon | | | Temperature | | | Pressure | | | Relative humidity | | |
|---|---|---|---|---|---|---|---|---|---|---|---|---|---|
| | | Hall A | Hall B | Hall C | Hall A | Hall B | Hall C | Hall A | Hall B | Hall C | Hall A | Hall B | Hall C |
| | Hall A | 1.00 | | | | | | | | | | | |
| $Rn_i$ | Hall B | 0.98 | 1.00 | | | | | | | | | | |
| | Hall C | 0.96 | 0.94 | 1.00 | | | | | | | | | |
| | Hall A | − 0.13 | − 0.07 | − 0.16 | 1.00 | | | | | | | | |
| $T_i$ | Hall B | 0.09 | 0.18 | 0.05 | 0.53 | 1.00 | | | | | | | |
| | Hall C | − 0.02 | 0.09 | − 0.03 | 0.32 | 0.86 | 1.00 | | | | | | |
| | Hall A | 0.11 | 0.13 | 0.11 | 0.14 | 0.12 | 0.06 | 1.00 | | | | | |
| $P_i$ | Hall B | 0.14 | 0.13 | 0.13 | 0.07 | 0.01 | − 0.10 | 0.97 | 1.00 | | | | |
| | Hall C | 0.10 | 0.12 | 0.15 | 0.07 | 0.10 | 0.09 | 0.97 | 0.94 | 1.00 | | | |
| | Hall A | 0.73 | 0.69 | 0.69 | − 0.14 | 0.22 | 0.05 | 0.34 | 0.37 | 0.36 | 1.00 | | |
| $RH_i$ | Hall B | 0.72 | 0.68 | 0.67 | 0.00 | 0.12 | − 0.12 | 0.35 | 0.41 | 0.33 | 0.96 | 1.00 | |
| | Hall C | 0.70 | 0.67 | 0.70 | 0.01 | 0.17 | − 0.07 | 0.36 | 0.41 | 0.38 | 0.96 | 0.98 | 1.00 |

and the $^{222}$Rn concentration, $r = 0.7$, for the nine pairs of the three halls. There exists a hint of a minor correlation between the relative humidity and the pressure, with $r$ close to 0.39. The other pairs are not significantly correlated.

The seasonal periodicity of the relative humidity and the $^{222}$Rn concentration produces the here reported correlation between both parameters in the three halls (Table 2 and Fig. 4). The seasonal periodicity is not observed either for the atmospheric pressure or the room temperature (Fig. 2) because the former is determined by the external atmospheric pressure (non seasonal, see Sect. 4) and the latter depends, mainly, on the internal air conditioning system and, sometimes, on considerable local alterations.

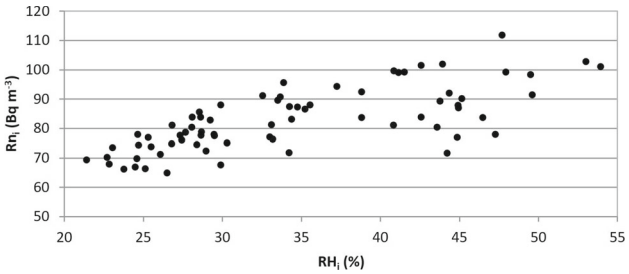


**Fig. 4** Monthly averages of the $^{222}$Rn concentration versus the monthly averages of the relative humidity at hall A from 2013 to 2018. Corresponding plots for halls B and C are similar

### 3.2 Seasonal periodicity of the $^{222}$Rn concentration and of the relative humidity inside the laboratory

The airborne radon depends on the radon concentration in soil gases and on its release to the atmosphere. A long-term study on the effects of climate on soil radon [35] found that wind speed, relative humidity, air and soil temperatures, and the difference between those temperatures cause both day-to-day and seasonal variations in soil radon, being seasonal variations of greater magnitude than day-to-day fluctuations. Although meteorological variables are not independent and it is difficult to estimate their relative impact, the authors of reference [35] were able to conclude that precipitation appears to be the most important meteorological variable affecting the content and the seasonal variation of $^{222}$Rn in soil gases.

**Table 3** Values of the fitted parameters of the relative humidity of the years 2013–2018 to Eq. (2). The maxima are in the first week of August

| Room | A (%) | B (%) | T (days) | $t_M$ (days) |
|---|---|---|---|---|
| Hall A | $34.6 \pm 0.4$ | $11.2 \pm 0.6$ | $364 \pm 2$ | $214 \pm 5$ |
| Hall B | $41.8 \pm 0.5$ | $11.7 \pm 0.7$ | $363 \pm 2$ | $217 \pm 6$ |
| Hall C | $40.2 \pm 0.5$ | $12.0 \pm 0.7$ | $364 \pm 2$ | $215 \pm 6$ |

Differences between summer and winter $^{222}$Rn concentration have been reported in large dwellings samples [36,37]. The general trend is that indoor $^{222}$Rn is higher in winter than in summer (winter/summer ratio, W/S $> 1$); we have observed in LSC the opposite result. However, the dispersion of the measurements in [36,37] is significant and there exist values of W/S $< 1$. Other observations of W/S $< 1$ have also been reported, see [38] and references therein; on the other hand, the result of [39] shows that W/S $> 1$ for indoor $^{222}$Rn, whereas W/S $< 1$ for outdoor $^{222}$Rn. A quantitative model [40] provides a sinusoidal variation in the monthly average of the indoor $^{222}$Rn concentration with W/S $> 1$, but the model also shows that the maximum $^{222}$Rn concentration occurs in summer (W/S $< 1$) if the building materials are the dominant radon source.

The annual periodicity of the relative humidity and the concentration of $^{222}$Rn at LSC can be analyzed fitting the values of their monthly average to an equation of the type

$$Y = A + B\cos\left(\frac{2\pi(t - t_M)}{T}\right) \tag{2}$$

where $A$ and $B$ are the annual average and the modulation amplitude, respectively, $T$ is the period, $t_M$ is the time corresponding to the first maximum amplitude and $t$ is the measurement time after 1 January 2013 at 00:00.

The parameters $A$, $B$, $T$ and $t_M$ are estimated by an unweighted least squares fit because the standard deviations of the measurements of the relative humidity and radon concentration are unknown. This is the typical situation of parameters having a natural variability not linked to the statistical uncertainty of the measurement. Therefore, the standard deviation of each measurement is estimated *a posteriori*, assuming that it is the same for each measurement of the fit, using the square root of the minimum of the sum of the squared residuals per degree of freedom [41]. The results for the relative humidity are listed in Table 3. The three periods are compatible with 1 year and the three maxima $t_M$ are equal (within uncertainties), their mean value is $215 \pm 3$ day, around 3 August.

The concentrations of $^{222}$Rn were also fitted to the Eq. (2). Table 4 shows the values of the fitted parameters. The unweighted least squares fits show that the estimated standard deviations of the measurements are 7.6, 7.6 and 8.0 Bq m$^{-3}$

**Table 4** Values of the fitted parameters of the $^{222}$Rn concentration of the years 2013–2018 to Eq. (2). The maxima are in mid-July

| Room | A (Bq m$^{-3}$) | B (Bq m$^{-3}$) | T (days) | $t_M$ (days) |
|---|---|---|---|---|
| Hall A | $82.8 \pm 0.9$ | $10.6 \pm 1.3$ | $366 \pm 4$ | $194 \pm 12$ |
| Hall B | $85.2 \pm 0.9$ | $10.0 \pm 1.3$ | $368 \pm 4$ | $193 \pm 13$ |
| Hall C | $84.8 \pm 0.9$ | $9.8 \pm 1.3$ | $367 \pm 5$ | $189 \pm 14$ |

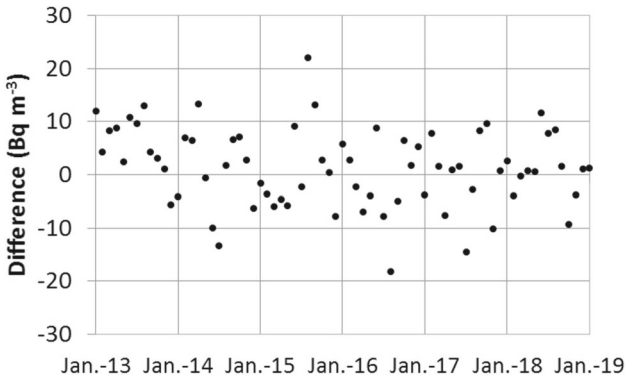


**Fig. 5** Differences between the experimental and the fitted values of $^{222}$Rn concentration of hall A to Eq. (2). Corresponding plots for halls B and C are similar

for the halls A, B and C, respectively. These values imply a mean standard deviation of 9% for the $^{222}$Rn concentration monthly averages, a value much greater than their statistical uncertainty according to the monitor response (0.24%, see Sect. 3). Therefore, the observed $^{222}$Rn monthly deviation from annual modulation is not linked to the measurement precision, but to the natural variability of the $^{222}$Rn at the mountain where the fresh air is taken.

The differences between the observed and the fitted values do not show any particular trend (Fig. 5). Most of the differences are less than 10 Bq m$^{-3}$ and their maximum is 20 Bq m$^{-3}$. Therefore, the sinusoidal function is a reasonable model. As in the case of the humidity, the three maxima, $t_M$, are compatible within their uncertainties, giving a mean value of $192 \pm 8$ days, around 11 July. This means that the $^{222}$Rn maxima (minima) occur $23 \pm 8$ days before the humidity maxima (minima).

The origin of the winter-summer $^{222}$Rn level difference can be attributed to the different conditions of the airflow and weather patterns. There exist different features of the $^{222}$Rn concentration in different laboratories. For instance, the annual periodicity has not been observed in the Laboratori Nazionali del Gran Sasso (LNGS) [2], which is connected to a road tunnel in Italy, under the Gran Sasso mountain. On the contrary, the periodicity has been observed in the Soudan Underground Laboratory (SUL) [42], located in an old iron mine in Minnesota, with the maximum in summer and the minimum in winter, as we report in LSC. However, as the

**Table 5** Altitude and coordinates of the LSC and of the AEMET stations used in this work. The stations data were provided by AEMET; those of LSC are our estimates on the application iberpix [44] of the Spanish National Geographic Institute (Instituto Geográfico Nacional)

| Site | Altitude (m) | Latitude | Longitude |
|---|---|---|---|
| LSC | 1120 | 42° 46′ 30″ N | 0° 31′ 42″ W |
| Canfranc | 1170 | 42° 44′ 58″ N | 0° 30′ 58″ W |
| Aragüés del Puerto | 1040 | 42° 42′ 32″ N | 0° 40′ 23″ W |

relative humidity in SUL is constant, it is not correlated to the $^{222}$Rn concentration inside the laboratory [43].

It was suggested in [42] that the radon periodicity in the SUL is due to the temperature difference between the air in the mine and that on the surface because the hot air raises: in winter, when the outside temperature is lower than the inside one, the ventilation rate is enhanced and the purge of the inside radon is more efficient than in summer, when the temperature gradient is reduced or, even, reversed. This qualitative model can also be applied to LSC. Then, the $^{222}$Rn concentration has a positive correlation with the outside temperature and the winter-summer ratio, W/S, inside the laboratory is less than one. The observed positive correlation between the radon level and the relative humidity inside the LSC is of indirect origin. It can be explained because in winter the rock of the tunnel contains less water than in summer, when the snow had melted mostly well before and the rock is plenty of water. In these conditions, the relative humidity inside the laboratory is greater in summer than in winter. Therefore, the high (low) humidity inside LSC is a consequence of the high (low) outside temperature.

## 4 Meteorological data

A quantitative estimate of the positive correlation between the $^{222}$Rn concentration and the temperature outside the laboratory can be obtained from the data provided by the Spanish Meteorological Agency (Agencia Española de Meteorología, AEMET).

The nearest AEMET observation point to the LSC is the Canfranc station, 3 km away from the underground laboratory. It records the temperature ($T_o$) and relative humidity ($RH_o$) every 10 min. The Aragüés del Puerto station, 13 km away, records the atmospheric pressure ($P_o$) four times per day: midnight, 7:00, 12:00 and 18:00 hours. Table 5 lists the altitudes and coordinates of LSC and both AEMET stations.

We use data from 2015 to 2018 because the meteorological Canfranc data are available since the end of October, 2014. The correlation coefficients between the inside (four) and outside (three) studied variables from 2015 to 2018 for the three halls of the LSC are listed in Table 6. In this case with 36 evaluated $r$-values, we use 99.86% CL for the decision threshold because $1-(0.9986)^{36}=0.05$, see Sect. 3.1. The monthly average 4-year data gives $n=48$ in Eq. (1), i.e., 46 degrees of freedom for the Student's $t$ and $|r_{\alpha=0.0014}|=0.46$.

**Table 6** Correlation coefficients (2015–18) between the four inside variables, recorded underground by our radon monitors, for the halls A, B and C of LSC and the outside variables recorded by the AEMET stations of Canfranc (temperature and relative humidity) and Aragüés del Puerto (pressure)

| Room | Outside variables | | |
|---|---|---|---|
| Hall A | $T_o$ | $P_o$ | $RH_o$ |
| $Rn_i$ | 0.71 | 0.10 | − 0.10 |
| $T_i$ | 0.14 | − 0.01 | − 0.20 |
| $P_i$ | 0.38 | 0.99 | − 0.40 |
| $RH_i$ | 0.95 | 0.25 | − 0.25 |
| Hall B | $T_o$ | $P_o$ | $RH_o$ |
| $Rn_i$ | 0.68 | 0.09 | − 0.08 |
| $T_i$ | 0.28 | − 0.14 | 0.32 |
| $P_i$ | 0.32 | 0.97 | − 0.36 |
| $RH_i$ | 0.94 | 0.29 | − 0.34 |
| Hall C | $T_o$ | $P_o$ | $RH_o$ |
| $Rn_i$ | 0.64 | 0.09 | − 0.16 |
| $T_i$ | 0.10 | − 0.15 | 0.31 |
| $P_i$ | 0.39 | 0.99 | − 0.40 |
| $RH_i$ | 0.94 | 0.28 | − 0.36 |

Independently of the hall, we observe three main features regarding the correlations inside-outside. First, the atmospheric pressures inside and outside are the variables with the highest correlation, $r\approx 1$, because the pressure gradient between two close points (13 km away and 80 m altitude difference) is constant (Fig. 7, bottom right panel). Second, the inside relative humidity and the outside temperature are highly correlated, $r=0.94$, most likely linked to the thaw season because the outside temperature follows a sinusoidal curve of 1-year period (Fig. 7) driving the inside relative humidity (Fig. 2). Note also that the outside relative humidity (Fig. 7) is not a sinusoidal curve similar to the inside relative humidity. Third, the inside $^{222}$Rn concentration is correlated with the outside temperature (Fig. 6), $r=0.64$ to $r=0.71$, a similar amount to the correlation between the inside $^{222}$Rn concentration and the inside relative humidity, $r=0.67$ to $r=0.73$ (Table 2). Latter correlation occurs in the same hall and also for different halls.

The Table 7 collects the results of fitting $T_o$, $RH_i$, and $Rn_i$ to Eq. (2) within the same interval of available data for $T_o$ (2015–2018). $T_o$ has a period compatible with 1 year and the maximum is $204\pm 3$ days, around 23 July. The period of

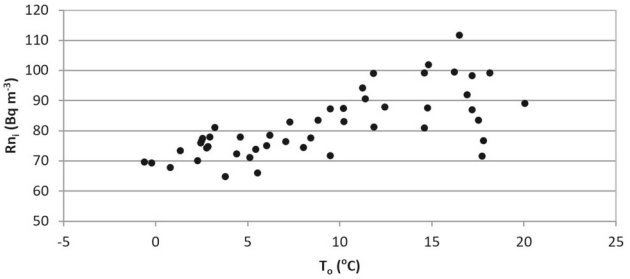


**Fig. 6** Monthly averages of the $^{222}$Rn concentration at hall A versus the monthly averages of the outside temperature from 2015 to 2018. Corresponding plots for halls B and C are similar

the internal relative humidity, $RH_i$, is also compatible with one year and the maxima $t_M$ in every hall are equal within uncertainties, their mean value is $213 \pm 3$ days, around 1 August, $9 \pm 5$ days after the maximum of $T_o$. Though this delay has a low statistical significance, it could be a rough estimate of the time interval between the maximum thaw on the Tobazo Mountain and the maximum rock humidity at 800 m rock depth. The $^{222}$Rn results of the 2015–2018 series for the three halls show a period compatible with 1 year and a maximum $10 \pm 14$ days after the maximum of $T_o$. Compared to the 2013–2018 series (Table 4), the subset 2015–2018 exhibits differences in the estimated parameters (the most remarkable are $\sim$ 10 days in the period values and $\sim$ 3 weeks in the $t_M$ values). In this subset the $^{222}$Rn maxima (minima) occur at the same time the humidity maxima (minima), whereas in the total set 2013-2018 they occur $23 \pm 8$ days before (see Sect. 3.2). This behaviour appears because the seasonal periodicity of the $^{222}$Rn concentration has more fluctuations than the one of the relative humidity, see the fits of the Fig. 2, because it is more sensitive to variations in the environmental conditions; for instance, the outside rainfall changes the radon content of the fresh air cleaning the laboratory, but it does not change the relative humidity inside the laboratory, 800 m down in the rock.

## 5 $^{222}$Rn control in the ANAIS-112 experiment

The $^{222}$Rn annual periodicity in the hall B of LSC was also reported by the ANAIS collaboration [45], an experiment looking for the dark matter annual modulation with NaI(Tl) scintillators at LSC [11,12,46,47] to test the DAMA-LIBRA result [48] using the same target and experimental approach. To keep low the concentration of $^{222}$Rn, the air inside the ANAIS-112 shielding has been kept continuously flushed with radon-free nitrogen gas. During most of the ANAIS-112 operation this radon-free nitrogen gas has been produced

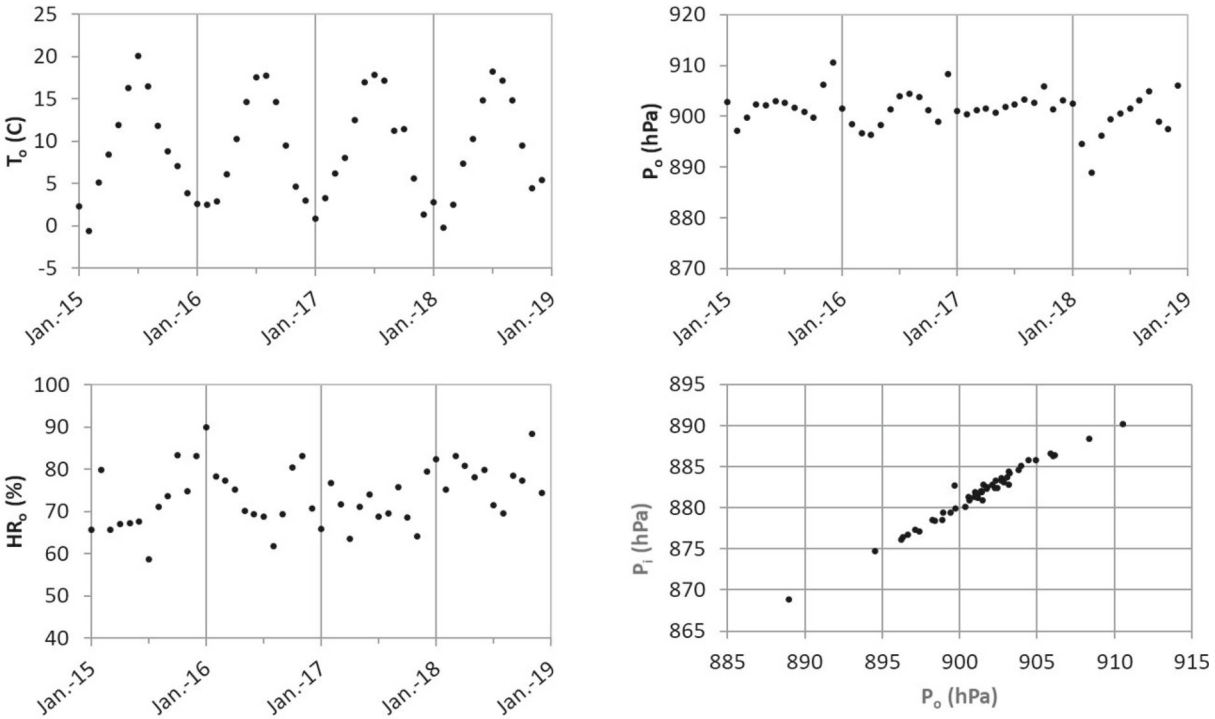


**Fig. 7** Monthly averages of AEMET meteorological data: temperature (upper left), pressure (upper right) and relative humidity (bottom left). The bottom right panel shows the high correlation between the atmospheric pressures in hall A ($P_i$) and Aragüés del Puerto ($P_o$); halls B and C have similar correlation with $P_o$

**Table 7** Values of the fitted parameters (2015–18) according Eq. (2) of the variables showing seasonal periodicity: outside temperature (maximum on 23 July), inside relative humidity and inside radon concentration (maxima on beginning August)

| Outside temperature | | | | |
|---|---|---|---|---|
| | A (°C) | B (°C) | T (days) | $t_M$ (days) |
| Canfranc | $9.1 \pm 0.2$ | $8.1 \pm 0.3$ | $366 \pm 2$ | $204 \pm 3$ |
| Inside relative humidity | | | | |
| | A (%) | B (%) | T (days) | $t_M$ (days) |
| Hall A | $33.9 \pm 0.4$ | $11.1 \pm 0.5$ | $361 \pm 2$ | $218 \pm 4$ |
| Hall B | $40.5 \pm 0.5$ | $11.9 \pm 0.7$ | $365 \pm 3$ | $210 \pm 6$ |
| Hall C | $39.3 \pm 0.5$ | $12.2 \pm 0.7$ | $367 \pm 3$ | $208 \pm 6$ |
| Inside $^{222}$Rn concentration | | | | |
| | A (Bq m$^{-3}$) | B (Bq m$^{-3}$) | T (days) | $t_M$ (days) |
| Hall A | $82.0 \pm 1.1$ | $11.2 \pm 1.5$ | $357 \pm 7$ | $214 \pm 13$ |
| Hall B | $84.9 \pm 1.1$ | $10.4 \pm 1.5$ | $358 \pm 7$ | $215 \pm 14$ |
| Hall C | $84.4 \pm 1.1$ | $10.3 \pm 1.5$ | $358 \pm 8$ | $214 \pm 14$ |

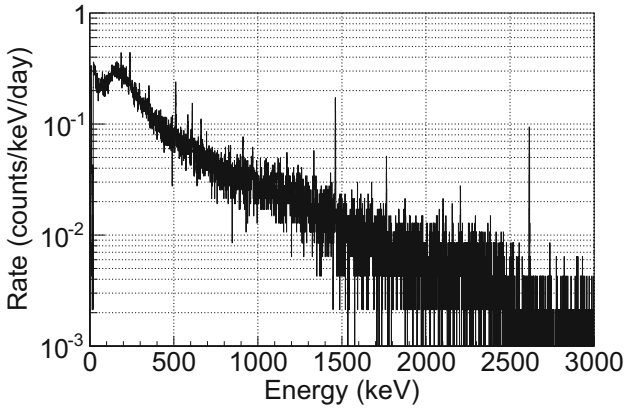


**Fig. 8** Total HPGe spectrum for 2017–2018 (670 days live time)

by evaporating liquid nitrogen, but also pure nitrogen from compressed gas bottles has been used. Throughout 2017 and 2018 (commissioning runs and the first one and a half years of data) we purged the inner volume ($20 \times 20 \times 30$ cm$^3$) of the shielding [49] of a HPGe detector ($\sim$1 kg) with the same gas purging the ANAIS-112 shielding. This monitoring was used to crosscheck the steady acquisition rate of ANAIS-112 and to discard any annual modulation coming from the radon in the laboratory. As a byproduct we obtained an upper limit to the residual $^{222}$Rn concentration in air, because our data cannot separate the $^{222}$Rn contribution from those of $^{226}$Ra and $^{238}$U in the shielding or in the HPGe. The total spectrum (670 days live time) is plotted in Fig. 8.

The efficiency to the $^{222}$Rn source was estimated in two steps. First, the relative efficiency, $\epsilon_R(E)$, of the HPGe to the $^{222}$Rn was measured profiting the airborne $^{222}$Rn filling

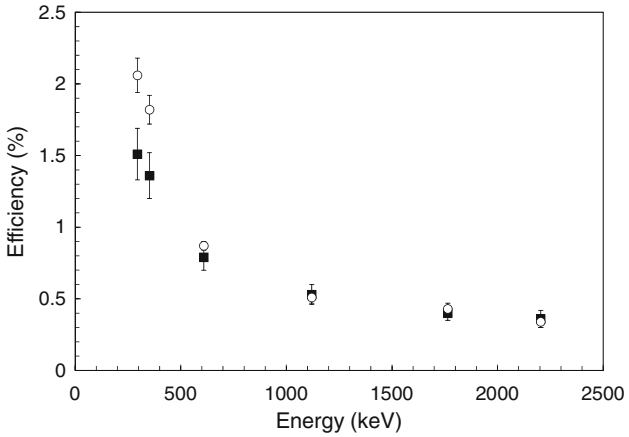


**Fig. 9** Efficiency of our HPGe detector to a $^{222}$Rn source filling the inner volume of its shielding. The squares were estimated profiting a $^{222}$Rn efficiency relative measurement and the circles using Geant4 with an approximate geometry. In both cases the estimated values were normalized to the measured efficiency at 1460.8 keV

the inner volume of the shielding due to an accidental cut of the purging system. Second, we measured the efficiency at 1460.8 keV, $\epsilon$(1460.8 keV), using a source of 260 g of KCl located at several positions in the accessible volume around the HPGe, and another one of 20.6 g at several distances from the HPGe window. We have estimated a 10% systematic uncertainty for $\epsilon$(1460.8 keV) because the lack of measurements for sources located at the rear of the HPGe. The normalization of $\epsilon_R$(1460.8 keV) to the measured $\epsilon$(1460.8 keV) gives the efficiencies for the $^{222}$Rn gamma lines (Fig. 9). A Monte Carlo simulation with Geant4 [50] according to the known geometry of the HPGe detector agrees with the former from 0.6 to 2.2 MeV (Fig. 9). The differences at low energy are due to the partial knowledge of the geometry.

The best upper limit, 0.06 Bq m$^{-3}$ (95% C.L.), is obtained with the 351.9 keV gamma line. This value is one order of magnitude better than our previous estimate based on the NaI(Tl) data [51,52]. According to the ANAIS-112 background model [52], this upper limit means that the contribution of the $^{222}$Rn to the total rate is $< 4 \times 10^{-4}$ counts keV$^{-1}$kg$^{-1}$d$^{-1}$ in the region of interest, [1–6] keV, amounting to less than 0.01% of the background [12].

The possible contribution of some modulation of some tiny $^{222}$Rn activity to the expected signal in ANAIS-112 is negligible because if we would take the above upper limit of 0.06 Bq m$^{-3}$ as a true $^{222}$Rn concentration with a modulation amplitude $\sim$ 10%, similar to the one observed in the hall B (Table 4), its contribution to the ANAIS-112 modulation signal would be $4 \times 10^{-5}$ counts keV$^{-1}$kg$^{-1}$d$^{-1}$ in the region [1–6] keV, much below the modulation observed by the DAMA/LIBRA collaboration [48] and the sensitivity of ANAIS-112 experiment [53].

Once ANAIS-112 had collected more than one year data, the laboratory installed and commissioned a radon abatement system (RAS) that can provide 220 $m^3\,h^{-1}$ with $\sim$1 mBq $m^{-3}$ of $^{222}$Rn for the experiments hosted by the LSC [6]. Though this $^{222}$Rn concentration is very low to be detected by our HPGe detector, we have monitored the air from the RAS from January, 2019 to June, 2021; adding up to 728 days live time. We have not observed significant differences between this measurement and the one done with evaporated nitrogen and we have obtained the same upper limit, 0.06 Bq $m^{-3}$ (95% C.L.), to the $^{222}$Rn around our HPGe detector.

## 6 Conclusions

The measurements performed at the LSC over 6 years (2013–2018) have shown that the monthly average $^{222}$Rn concentration in air is lower than the maximum allowed for working places, 600 Bq $m^{-3}$, according to the Spanish legislation [30] and the international recommendations [29]. It is essentially similar in the three experimentation halls at LAB2400 (see Table 1), indicating that the heating and the forced ventilation of the air reaching the LSC halls work properly.

There is a correlation between the $^{222}$Rn concentration and the relative humidity in the three halls. An annual and sinusoidal periodicity of the values of the relative humidity and the $^{222}$Rn concentration was observed in the three halls. The data from 2013 to 2018 show that the maximal humidity inside LSC occurs at beginning August and the maximal $^{222}$Rn concentration occurs 3 weeks before, at mid-July. The relative amplitude of the $^{222}$Rn concentration with respect to the annual average is about 10% for the three halls. According to the AEMET data used in this work, the $^{222}$Rn concentration is correlated with the temperature of the fresh air intake on the mountain covering the LSC. The correlation with the relative humidity inside LSC is indirect, because of the likely correlation between the external temperature and the internal humidity via the snow melting.

The low $^{222}$Rn content, $< 0.06$ Bq $m^{-3}$ (95% C.L.), of the nitrogen purging the ANAIS-112 shielding does not affect to the achieved low background and it guarantees the sensitivity of the experiment. The same upper limit was obtained after monitoring the air from the RAS, concluding that both systems are equivalent at this level of $^{222}$Rn sensitivity.

**Acknowledgements** This research was funded by MCIN/AEI/10.13039/501100011033 under Grant PID2019-104374GB-I00; by MINECO-FEDER under Grants FPA2017-83133-P, and FPA2014-55986-P; by MICINN-FEDER under Grants FPA2011-23749; by CONSOLIDER-Ingenio 2010 Programme under Grants MultiDark CSD2009-00064 and CPAN CSD2007-00042; by the University of Zaragoza under Grant UZ2017-CIE-09; by the Spanish Meteorological Agency (AEMET), the Gobierno de Aragón (Group in Nuclear and Astroparticle Physics, ARAID Foundation and I. Coarasa predoctoral grant), the European Social Fund and by the LSC consortium. The authors would like to acknowledge the use of Servicio General de Apoyo a la Investigación-SAI, Universidad de Zaragoza. The authors also thank Carlos Peña-Garay, Director of the LSC, Aldo Ianni and Alessandro Bettini (former LSC Directors) and José Ángel Villar (former LSC Associate Director) for their support and encouragement.

**Data Availability Statement** This manuscript has no associated data or the data will not be deposited. [Authors' comment: Meteorological data belongs to AEMET and data taken inside the laboratory belongs to the Canfranc Underground Laboratory. Both sets can be made available on reasonable request with the corresponding permissions of AEMET or the Canfranc Underground Laboratory.]


Funded by SCOAP$^3$. SCOAP$^3$ supports the goals of the International Year of Basic Sciences for Sustainable Development.

## References

1. C. Arpesella, et al., Health Phys. **72**(4), 629 (1997). https://journals.lww.com/health-physics/Fulltext/1997/04000/Radon_Measurements_in_the_Gran_Sasso_Underground.16.aspx
2. A. Bassignani, et al., Radiat. Meas. **28**(1), 609 (1997). International Conference on Nuclear Tracks in Solids. https://doi.org/10.1016/S1350-4487(97)00151-0
3. K.T. Lesko, Phys. Procedia **61**, 542 (2015). 13th International Conference on Topics in Astroparticle and Underground Physics, TAUP 2013. https://doi.org/10.1016/j.phpro.2014.12.001
4. C. Liu, et al. Measurements of Radon Concentrations Using CR-39 Detectors in China JinPing Underground Laboratory (2015–2016) (2018). arXiv:1806.06567
5. G. Cinelli, M. De Cort, T. Tollefsen (eds.), *European Atlas of Natural Radiation* (Publication Office of the European Union, Luxembourg, 2019)
6. J. Perez-Perez et al., Universe **8**(2) (2022). https://doi.org/10.3390/universe8020112
7. M. Stein et al., Nucl. Instrum. Methods Phys. Res. Sect. A Accelerators Spectrom. Detectors Assoc. Equip. **880**, 92 (2018). https://doi.org/10.1016/j.nima.2017.10.054
8. A.K. Drukier, K. Freese, D.N. Spergel, Phys. Rev. D **33**, 3495 (1986). https://doi.org/10.1103/PhysRevD.33.3495
9. M. Lee et al., J. Korean Phys. Soc. **58**(4), 713 (2011). https://doi.org/10.3938/jkps.58.713
10. P. Adamson et al., Phys. Rev. D **87**, 032005 (2013). https://doi.org/10.1103/PhysRevD.87.032005
11. J. Amaré et al., Eur. Phys. J. C **79**(3), 228 (2019). https://doi.org/10.1140/epjc/s10052-019-6697-4
12. J. Amaré et al., Phys. Rev. D **103**, 102005 (2021). https://doi.org/10.1103/PhysRevD.103.102005
13. E. Sanchez Garcia, J. Instrum. **15**(02), C02044 (2020). https://doi.org/10.1088/1748-0221/15/02/c02044

14. I.C. Bandac et al., J. High Energy Phys. **2020**(1), 18 (2020). https://doi.org/10.1007/JHEP01(2020)018
15. C. Adams et al., J. High Energy Phys. **2021**(8), 164 (2021). https://doi.org/10.1007/JHEP08(2021)164
16. J. Castel et al., Eur. Phys. J. C **79**(9), 782 (2019). https://doi.org/10.1140/epjc/s10052-019-7282-6
17. A. Abeln et al., J. High Energy Phys. **2021**(5), 137 (2021). https://doi.org/10.1007/JHEP05(2021)137
18. T. Martinez et al., Nucl. Instrum. Methods Phys. Res. Sect. A Accelerators Spectrom. Detectors Assoc. Equip. **906**, 150 (2018). https://doi.org/10.1016/j.nima.2018.07.087
19. N. Mont-Geli, et al. First results from the HENSA/ANAIS collaboration at the Canfranc Underground Laboratory (2022). arXiv:2111.12616
20. J. Amaré et al., J. Phys. Conf. Ser. **39**, 151 (2006). https://doi.org/10.1088/1742-6596/39/1/035
21. J.M. Carmona et al., Astropart. Phys. **21**(5), 523 (2004). https://doi.org/10.1016/j.astropartphys.2004.04.002.
22. D. Jordan, et al., Astropart. Phys. **42**, 1 (2013). https://doi.org/10.1016/j.astropartphys.2012.11.007 [Corrigendum: Astroparticle Physics 118, 102372 (2020)]
23. W.H. Trzaska et al., Eur. Phys. J. C **79**(8), 721 (2019). https://doi.org/10.1140/epjc/s10052-019-7239-9
24. I. Bandac, et al., Radioprotección **77**(XXI), 36 (2014). https://www.sepr.es/recursos/revista/pr77.pdf
25. C.V. Evans, L.S. Morton, G. Harbottle, Soil Sci. Soc. Am. J. **61**(5), 1440 (1997). https://doi.org/10.2136/sssaj1997.03615995006100050023x
26. A. Navas, J. Soto, J. Machín, Appl. Radiat. Isot. **57**(4), 579 (2002). https://doi.org/10.1016/S0969-8043(02)00131-8
27. J. Gutiérrez-Villanueva et al., *Intercomparación de monitores de gas radón en condiciones de campo* (Editorial Universidad de Cantabria, Santander, 2016)
28. Council directive 2013/59/EURATOM. Official Journal of the European Union, 17 January 2014, L13. https://eur-lex.europa.eu/eli/dir/2013/59/oj
29. International Commission on Radiological Protection, Ann. ICRP **37**(2–4), 1 (2007). https://www.icrp.org/publication.asp?id=ICRP
30. Consejo de Seguridad Nuclear, Madrid, *Guía de seguridad 11-04. Metodología para la evaluación de la exposición al radón en los lugares de trabajo* (2012). https://www.csn.es/en/guias-de-seguridad
31. L. Pujol, J. García Tobar, Revista Digital del Cedex **173**, 61 (2014). http://ingenieriacivil.cedex.es/index.php/ingenieria-civil/article/view/378
32. J. Calvo et al., J. Cosmol. Astropart. Phys. **2017**(03), 003 (2017). https://doi.org/10.1088/1475-7516/2017/03/003
33. A. Stuart, J.K. Ord, *Kendall's Advanced Theory of Statistics, Volume 1: Distribution theory*, 5th edn. (Griffin and Co, 1987). Sections 16.24 to 16.28
34. M. Kendall, A. Stuart, *The Advanced Theory of Statistics, Volume 2: Inference and Relationship*, 4th edn. (Griffin and Co, 1979). Sections 31.18 and 31.19
35. S. Asher-Bolinder, *Field Studies of Radon in Rocks, Soils, and Water*, 1st edn. (CRC Press, 1992). A Preliminary Evaluation of Environmental Factors Influencing Day-to-Day and Seasonal Soil-Gas Radon Concentrations, pp. 23–31
36. H. Arvela, Radiat. Prot. Dosim. **59**(1), 33 (1995). https://doi.org/10.1093/oxfordjournals.rpd.a082634
37. F. Bochicchio, et al., Radiat. Meas. **40**(2), 686 (2005). Proceedings of the 22nd International Conference on Nuclear Tracks in Solids.https://doi.org/10.1016/j.radmeas.2004.12.023
38. A.B. Tanner, *Field Studies of Radon in Rocks, Soils, and Water*, 1st edn. (CRC Press, 1992). Methods of characterization of ground for assessment of indoor radon potential at a site, pp. 1–18
39. J. Hans, R. Lyon, Seasonal variations of radon and radon decay product concentrations in single family homes. Technical report, U.S. Environmental Protection Agency (1986). EPA 520/1-86-015 report
40. H. Arvela, O. Holmgren, P. Hänninenc, Radiat. Prot. Dosim. **168**(2), 277 (2016). https://doi.org/10.1093/rpd/ncv182
41. P. Bevington, D. Keith, *Data Reduction and Error Analysis for the Physical Sciences*, 3rd edn. (Mc Graw Hill, Cambridge, 2002)
42. M.C. Goodman, in *26th International Cosmic Ray Conference* (1999). https://www.osti.gov/biblio/11872f
43. A. Tiwari, C. Zhang, D.M. Mei, P. Cushman, Phys. Rev. C **96**, 044609 (2017). https://doi.org/10.1103/PhysRevC.96.044609
44. https://www.ign.es/iberpix2/visor/. Accessed 17 Mar 2022
45. M.A. Oliván, Design, scale-up and characterization of the data acquisition system for the ANAIS dark matter experiment. Ph.D. thesis, Universty of Zaragoza (2016). https://zaguan.unizar.es/record/48118/files/TESIS-2016-078.pdf. Accessed 17 Mar 2022
46. J. Amaré et al., Phys. Rev. Lett. **123**, 031301 (2019). https://doi.org/10.1103/PhysRevLett.123.031301
47. J. Amaré et al., Eur. Phys. J. C **79**(5), 412 (2019). https://doi.org/10.1140/epjc/s10052-019-6911-4
48. R. Bernabei et al., Int. J. Mod. Phys. A **35**(36), 2044023 (2020). https://doi.org/10.1142/S0217751X20440236
49. I. Coarasa et al., J. Phys. Conf. Ser. **718**, 042049 (2016). https://doi.org/10.1088/1742-6596/718/4/042049
50. S. Agostinelli et al., Nucl. Instrum. Methods Phys. Res. Sect. A Accelerators Spectrom. Detectors Assoc. Equip. **506**(3), 250 (2003). https://doi.org/10.1016/S0168-9002(03)01368-8
51. S. Cebrián et al., Astropart. Phys. **37**, 60 (2012). https://doi.org/10.1016/j.astropartphys.2012.07.009
52. J. Amaré et al., Eur. Phys. J. C **76**(8), 429 (2016). https://doi.org/10.1140/epjc/s10052-016-4279-2
53. I. Coarasa et al., Eur. Phys. J. C **79**(3), 233 (2019). https://doi.org/10.1140/epjc/s10052-019-6733-4